Unsupervised Learning for Improved Gamma-ray Spectrometry in Pixelated Cadmium Zinc Telluride (CZT) Detectors

G. Aversano[a*], H. S. Parrilla[a], D. Hellfeld[a], and J. R. Vavrek[a]

[a]*Lawrence Berkeley National Laboratory, Berkeley, United States*

Mr. Gabriel Aversano, Lawrence Berkeley National Laboratory, 1 Cyclotron Road Mailstop 50C3396, Berkeley, CA, 94720, G.Aversano9@gmail.com

Unsupervised Learning for Improved Gamma-ray Spectrometry in Pixelated Cadmium Zinc Telluride (CZT) Detectors

Machine learning has been found ubiquitously useful across many industries, presenting an opportunity to improve radiation detection performance using data-driven algorithms. Improved detector resolution can aid in the detection, identification, and quantification of radionuclides. In this work, a novel, data-driven, unsupervised learning approach is developed to improve detector spectral characteristics by learning, and subsequently rejecting, poorly-performing regions of the pixelated detector. Feature engineering is used to fit individual characteristic photopeaks to a Doniach lineshape with a linear background model. Then, Principal Component Analysis (PCA) is used to learn a lower-dimension latent space representation of each photopeak where the pixels are clustered and subsequently ranked based on the cluster mean distance to an optimal point. Pixels within the worst cluster(s) are rejected to improve the Full Width Half Max (FWHM) by 10-15% (relative to the bulk detector) at 50% net efficiency when applied to training data obtained from measurements of a 100 μCi Europium-154 source using an H3D M400i pixelated Cadmium Zinc Telluride (CZT) detector. These results compare well with, but do not outperform, a greedy algorithm that accumulates pixels in order of FWHM from lowest to highest used as a benchmark. In the future, this approach can be extended to include the detector energy and angular response. Finally, the model is applied to newly seen natural and enriched uranium spectra relevant for nuclear safeguard applications.

Keywords: radiation detection, CZT, machine learning, unsupervised learning

1. INTRODUCTION

High-resolution pixelated Cadmium Zinc Telluride (CZT) gamma-ray detector systems have recently become an attractive technology and are commercially available from companies such as Michigan-based H3D Inc. In addition to excellent energy resolution (nominally <1% Full Width Half Max (FWHM) at 662 keV), modern CZT-based detectors can be operated at room temperature, are compact in size, have low power requirements, and can maintain good performance in high-flux environments [1]. CZT

detectors offer the operational benefits of low-resolution NaI(TI) scintillator detectors but improved performance of high-resolution High Purity Germanium (HPGe) detectors. These advantages have led to an increased interest in the adoption of CZT detectors for non-destructive nuclear material assay and gamma-ray spectrometry for nuclear safeguards applications [2].

The M400 detector system from H3D Inc. [3] now offers a high-resolution option with <0.65% FWHM at 662 keV for separated coincident interactions. However, to increase detection efficiency and therefore improve counting statistics, interactions are combined which ultimately degrades the energy resolution (<0.8% FWHM at 662 keV) due to spatially varying performance within the detector. Although care has been taken to properly normalize and align the spectra before summation [4], there remains a capability gap to automatically configure, combine, or cluster the pixelated detector to optimize the detector system performance. Specifically, poorly-performing pixels can be rejected to improve the spectral resolution at the cost of lower detector efficiency (and therefore longer measurement times). Since solving the true optimal detector segmentation by brute force is computationally intractable (2^{484} combinations), the use of machine learning algorithms is explored in this work.

Rapid development of machine learning algorithms has been found useful across various fields of study presenting an interesting opportunity for radiation detection performance improvements based on data-driven approaches without the need for improvements in detection hardware components. The area of unsupervised machine learning has become increasingly popular for pattern recognition tasks. The objective in unsupervised learning is to learn natural patterns within the data without the use of informative labels. One technique, known as dimensionality reduction, seeks to represent the data in a lower-dimension latent space where patterns are more apparent

[5]. Clustering is another unsupervised technique which seeks to cluster similar data into distinct groups to which the analyst can assign contextual meaning. Unsupervised learning may be useful for learning patterns within pixelated detectors to automatically cluster, and subsequently reject, poor-performing regions to improve the spectral performance by trading off lower detector efficiency. Improved spectral performance can aid in identification and assay of radiological sources in operational environments of interest for verification of nuclear material under nuclear safeguard applications. This approach is particularly effective for separating overlapping characteristic photopeaks where a reduction in detector efficiency with an improvement in resolution can reduce the peak area uncertainty.

Non-negative Matrix Factorization (NMF) [6] has been used to model gamma-ray spectra due to its ability to enforce non-negativity while remaining consistent with Poisson statistics. The NMF components, learned directly from measured gamma-ray data, are additive and physically interpretable. For example, NMF has proven successful in discovering physically relevant spectral structure from known sources such as terrestrial KUT and cosmic in gamma-ray background data [7]. Principal Component Analysis (PCA) [8] has been used for pulse-shape discrimination (PSD) of scintillation radiation detectors [9] and for anomaly detection of nuclear material [10]. PCA aims to find new principal components from the dataset in order of highest variation.

This work aims to utilize feature engineering (i.e., creating new information from the existing dataset) along with PCA and various clustering algorithms to cluster and subsequently reject detector pixels based on spectral performance. The approach is designed to be detector-agnostic and applicable to other pixelated detector systems such as segmented HPGe. The product of this effort will enable end users to span the

efficiency-resolution tradeoff in real-time in the field, ultimately improving the efficiency of routine nuclear safeguards techniques. The current work presents results for several single energy models. In the future, the feasibility of a single energy-agnostic model will be studied.

2. METHODOLOGY

2.1 Data Collection

Data was required to train the unsupervised learning algorithms to perform dimensionality reduction and clustering. Long-dwell (8 hour) measurements of a 100 μCi Eu-154 check source were obtained using the M400i[1] pixelated CZT detector [3] manufactured by H3D Inc. This source was chosen as it has several prominent photopeaks on the scale relevant to nuclear safeguard applications (in particular, 123 keV, 248 keV, 723 keV, and 1274 keV). The pixelated detector response is known to be energy dependent [4]. Thus, in future work, the wide range of energies could potentially be included as a higher dimensional input feature towards a single model. The check source was placed 40 cm from the detector at 12 locations chosen using the Hierarchical Equal Area isoLatitude Pixelization (HEALPix) library [11] to discretize the unit sphere into pixels with equal area. Measurements were obtained using a custom-built scanning system, illustrated in Fig. 1, capable of source placement anywhere in 4π with standoffs ranging from 30 – 160 cm. This experimental setup enabled the detector response to be characterized as a function of source energy and direction. However, in this work, the spectra from each source were averaged over the directional response of the detector before use in the unsupervised learning algorithm to simplify the problem by reducing

[1] The M400i detector includes a firmware update provided by H3D Inc. to enable full list-mode data including timestamped 3D position and energy event reconstruction.

the dimensionality. In future work, the 12 measurements can be used together to create a richer input feature to the model. Doing can enable either a direction-agnostic model or a model that can optimize the detector segmentation by incorporating the measurement direction. Although Eu-154 is used to train the algorithm, this model should be applicable to other isotopes relevant to nuclear safeguard applications. We utilize the model with never-before-seen uranium data to assert whether the model can generalize to new sources.

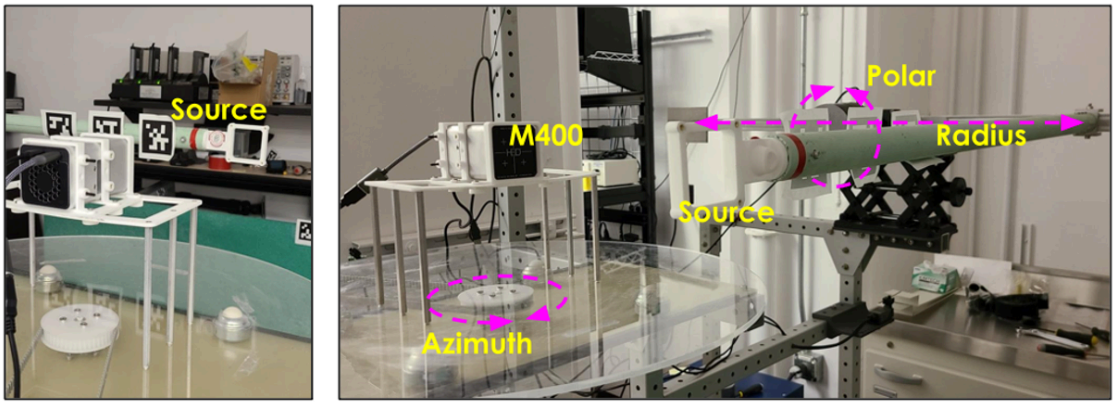

Figure 1. Experimental setup using Berkeley Lab scanning system capable of source placement anywhere in 4π with standoffs ranging from 30 – 160 cm.

The spectrum was collected in list mode, including 3D event position, and converted into binmode. Only single-site events were included in this analysis (which were estimated to cover >90% of all events). The M400i CZT detector contains 4 discrete crystals each with an 11x11 grid of pixels for a total of 484 pixels. The XY binning (1.9 mm) was determined by analyzing position differences in distinct horizontal and vertical lines of the collected data. Each pixel was also discretized into 50 virtual depth bins (0.2 mm) between the anode and cathode for a total of 24, 200 (484x50) voxels.

2.2 Feature Engineering

In this work, the CZT detector was discretized at the pixel level (i.e., the sum of virtual depth voxels). The spectral features for each pixel were obtained by fitting the counts in each of the four photopeaks of interest to a Doniach [12] lineshape parameterized by:

$$D(E) = \frac{A\cos\left[\frac{\pi\gamma}{2} + (1-\gamma)\left(\frac{E-\mu+\nu}{\sigma}\right)\right]}{\left(\sigma^2 + (E-\mu+\nu)^2\right)^{\frac{1-\gamma}{2}}} \quad (1)$$

$$\nu = \frac{2.3548\sigma}{2tan\left(\frac{\pi}{2-\gamma}\right)} \quad (2)$$

where A is the height (counts), μ is the centroid energy (keV), γ is the asymmetry (i.e., tailing) parameter (unitless), σ is the characteristic width parameter (keV) and E is the energy (keV). A linear background model was also included, resulting in a 6-parameter fit to each photopeak (Fig. 2).

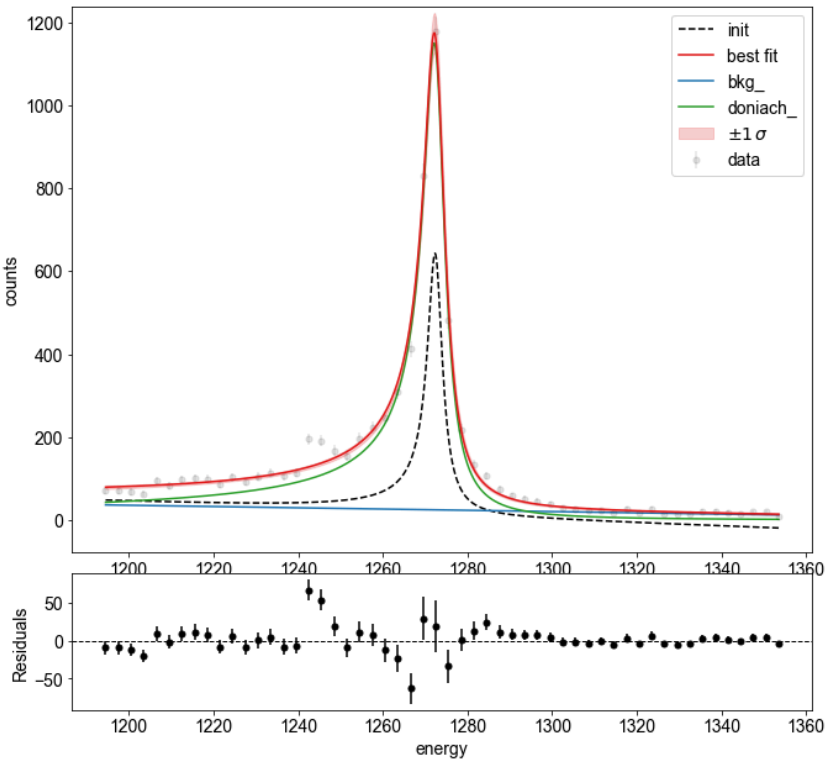

Figure 2. Feature engineering to map pixel counts to a 6-parameter fit that includes a Doniach lineshape plus a linear background (for a 1274 keV photopeak). The top sub-plot shows the raw counts with the best fit in red. The Doniach and background components of the best fit are shown in green and blue respectively. The bottom sub-plot shows the residuals between the raw counts and best fit.

The spectral features of the Eu-154 measurements were used as training data to the unsupervised learning algorithm to identify strongly- and poorly-performing regions of the detector. The amplitude feature was dropped to ignore rate differences between pixels (i.e., focus on lineshape). The centroid feature was also dropped as these spectra were recalibrated to have a consistent centroid (i.e., the detector can be calibrated). The remaining features were standardized to have a mean of zero and standard deviation of one. A separate single energy model was learnt for each of the four photopeaks of interest. Therefore, the input feature vector, X, used in the unsupervised learning model is $_{X \in R^{m \times n}}$ with $m = 484$ rows (pixels) and $n = 4$ columns (features).

2.3 Unsupervised Learning Model

The unsupervised learning model consists of two steps. First, PCA was used to project the spectral features into a lower-dimension latent space. Then, pixels were clustered using various clustering algorithms within the scikit-learn python package [13] including Birch [14], Agglomerative Clustering [15], K-Means [16], DBSCAN [17], OPTICS [18], Gaussian Mixture [19], AffinityPropagation [20], SpectralClustering [21], and MeanShift [22]. Although both NMF and PCA can be used for clustering, several other clustering algorithms that can perform better based on the distribution of the data and underlying patterns [23].

Although the input feature for a single energy model has low order, PCA was used to decompose the spectral features into a lower-dimension space to form the basis for future, multi-energy and/or multi-directional models of higher order. PCA aims to linearly transform the data into a set of the top k uncorrelated, orthogonal variables where $k < n$. These principal components are ranked in order of the highest variation. PCA diagonalizes the covariance vector, C, of input vector, X, to obtain the top k eigenvectors in V used to estimate X in lower order using Singular Value Decomposition (SVD):

$$C = \frac{X^T X}{n-1} \tag{3}$$

$$C = VLV^T \tag{4}$$

$$X \approx X_k = U_k S_k V_k^T \tag{5}$$

Next, the lower order representation of spectral features, X_k, was used to cluster pixels using various algorithms. In general, clustering algorithms seek to assign a cluster label to each data point typically grouping based on a distance or density metric or through expectation–maximization. For example, spectral clustering first performs an embedding on the dataset using a radial basis function (RBF) kernel and Gaussian Mixture clustering attempts to learn a mixed Gaussian Mixture Model from the dataset using an expectation-maximization algorithm to fit the models. In many cases, the number of clusters must be specified, motivating the need for a hyperparameter search.

2.3.1 Hyperparameters

The number of PCA latent features, k, was varied from $2 \leq k \leq 4$ for each single energy

model. The number of clusters, n, was varied from $2 \leq n \leq 10$. The default parameters (as per the scikit-learn package) were used for PCA and the following parameters were used for clustering: {'random_state': 42, 'max_iter': 500, 'tol': 1e-06, 'min_cluster_size': 250}. A grid search was used to find the optimal model hyperparameters from each of the 243 single energy models (3 lower dimension spaces (k) * 9 clustering algorithms * 9 number of clusters (n)).

2.4 Cluster Ranking

The Euclidean distance from the cluster mean to an 'optimal' location in the latent space was used to rank the clusters. This heuristic was chosen given that nearby pixels in the latent space should share key characteristics. The optimal location was chosen as the point in the latent space which produces the lowest Doniach sigma parameter ($\sigma > 0$) which, under a gaussian assumption, is proportional to the FWHM ($FWHM = 2\sqrt{2log(2)}\sigma$). The latent space was sampled with ten equally spaced points across each axis within the training data to locate the optimal point. Clusters were then ranked based on their Euclidean distance to this point.

For each model, pixels were accumulated by the best cluster and the average FWHM (normalized to the bulk detector) was computed to rank the models. The best model has the lowest average FWHM. This approach was chosen because the detector operator can trade off efficiency for resolution. However, there is likely an optimal efficiency-resolution trade off.

3. RESULTS & DISCUSSION

3.1 Detector Characterization

The FWHM varies considerably across pixels, shown in Fig. 3 and Fig. 4, motivating us

to remove poorly performing pixels to improve the detector resolution for some loss in detector efficiency. These plots reveal some trends across different energies: FWHM is worse around the edges of the detector for lower energies and in the center for higher energies, the bottom right crystal tends to perform worse across most energies, and FWHM is worse in general for lower energies. Characterization also revealed performance degradation as the source moved to the sides and behind the detector (likely due to self-shielding). This represents an opportunity for future work to include the source direction features as input to the unsupervised learning algorithm.

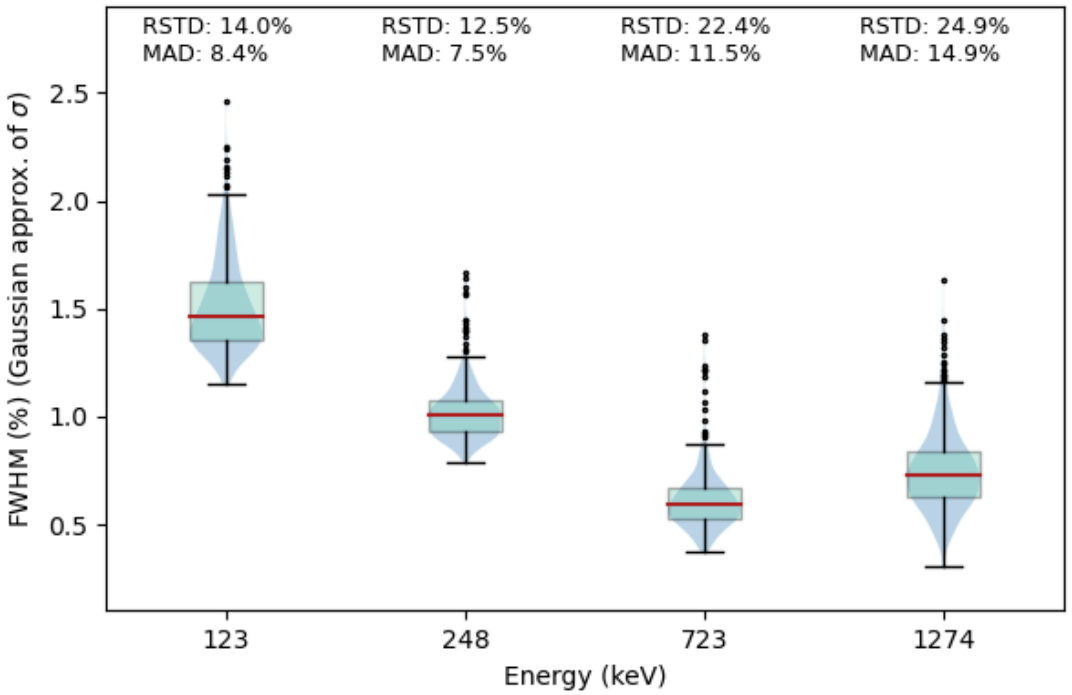

Figure 3. Distributions for four Eu-154 photopeaks (123 keV, 248 keV, 723 keV, and 1274 keV) by energy showing the variation in FWHM (%).

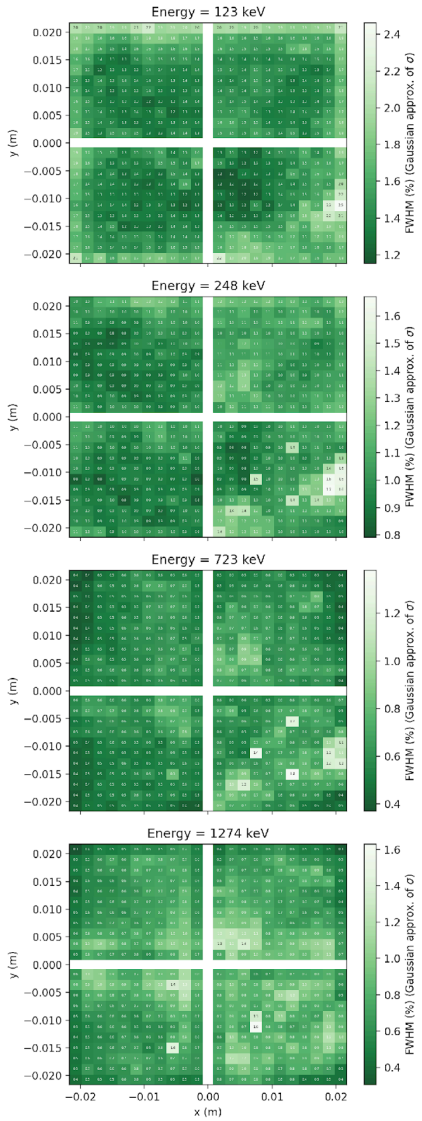

Figure 4. Distributions for four Eu-154 photopeaks (123, 248, 723. and 1274 keV) by pixel showing the variation in FWHM (%).

3.2 Pixel Latent Space, Clustering & Ranking

For each single energy photopeak, the spectral features were decomposed into a latent space and subsequently clustered using several algorithms. Clusters were ranked according to the Euclidean distance between the cluster mean and the optimal point within the latent space (see Fig. 5). Models were ranked according to the lowest cluster average FWHM (normalized to the bulk detector). The optimal hyperparameters were

found via grid search and are shown in Table 1.

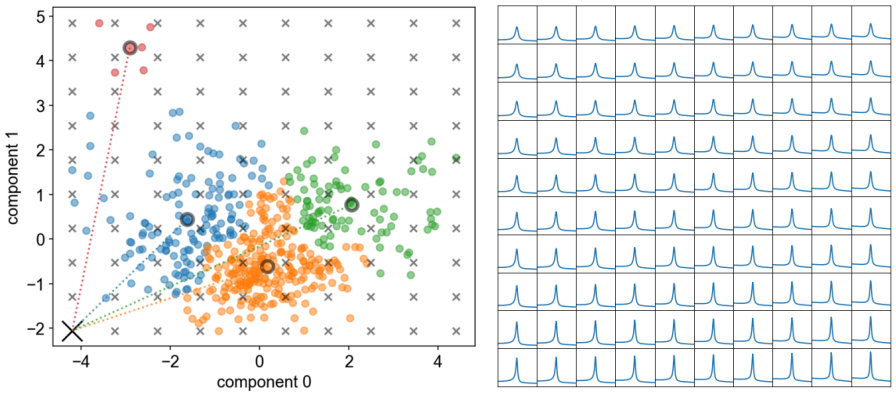

Figure 5. Two-component decomposition of individual pixel spectra fit-parameters (248 keV), shown as circles colored by cluster (left). The ranking metric (sigma) was sampled at the points marked by a small, grey x. The optimal point, based on the optimal sigma, is marked with a large, black X. The small, grey points were reconstructed back to the spectral space to show the Doniach lineshape (right).

Table 1. Optimal hyperparameters.

Energy (kev)	**PCA Components, k**	**Clustering Algorithm**	**# of Clusters, n**
123	4	Gaussian Mixture	3
248	2	Gaussian Mixture	3
723	4	Spectral	4
1274	3	Spectral	10

The worst clusters were subsequently removed and the FWHM for the remaining spectra was recalculated to quantify the performance improvement as a Figure of Merit (FoM) to the approach. For the best model, the ranking process was also completed at the pixel level by ranking pixels by distance to the optimal point in the latent space. Finally, as a baseline comparison, a greedy algorithm was used which ordered pixels

based on the individual FWHM. The relative FWHM vs net detector efficiency (i.e., with background subtraction) is shown in Fig. 6.

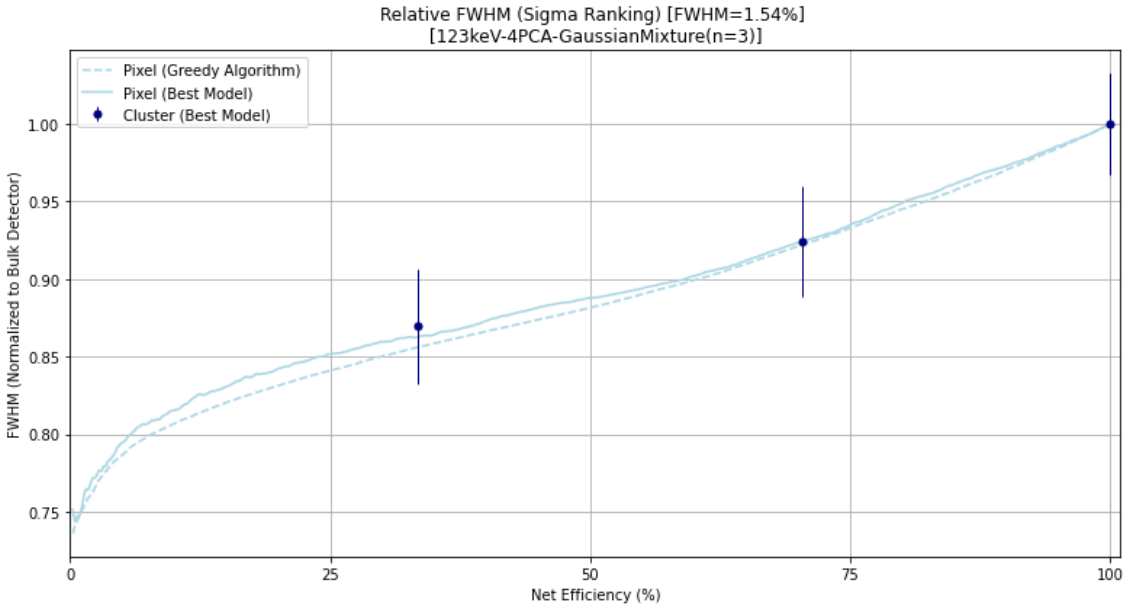

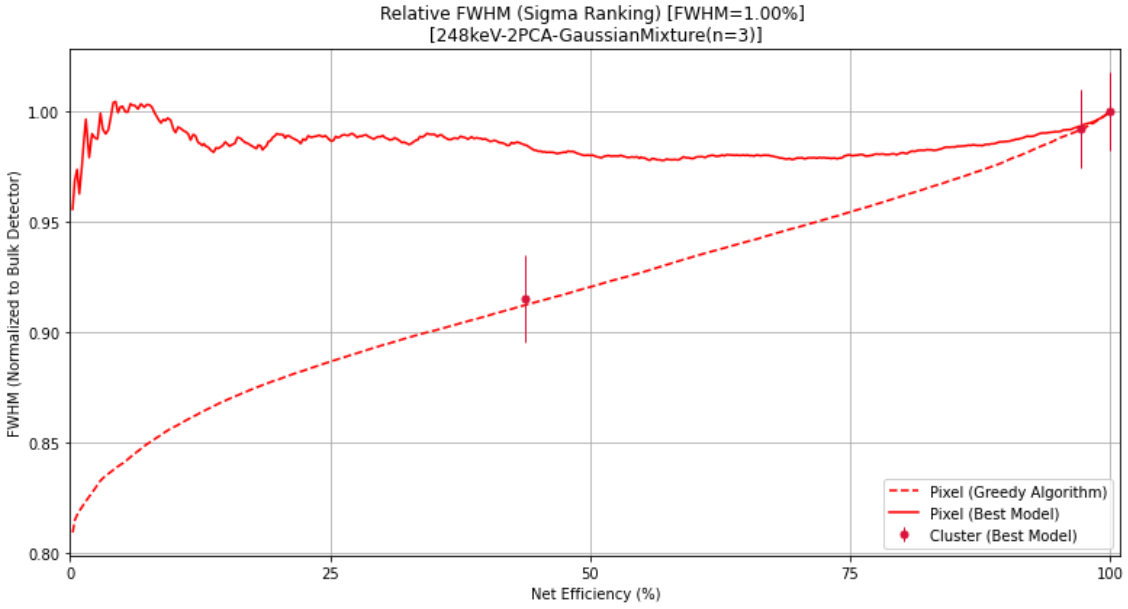

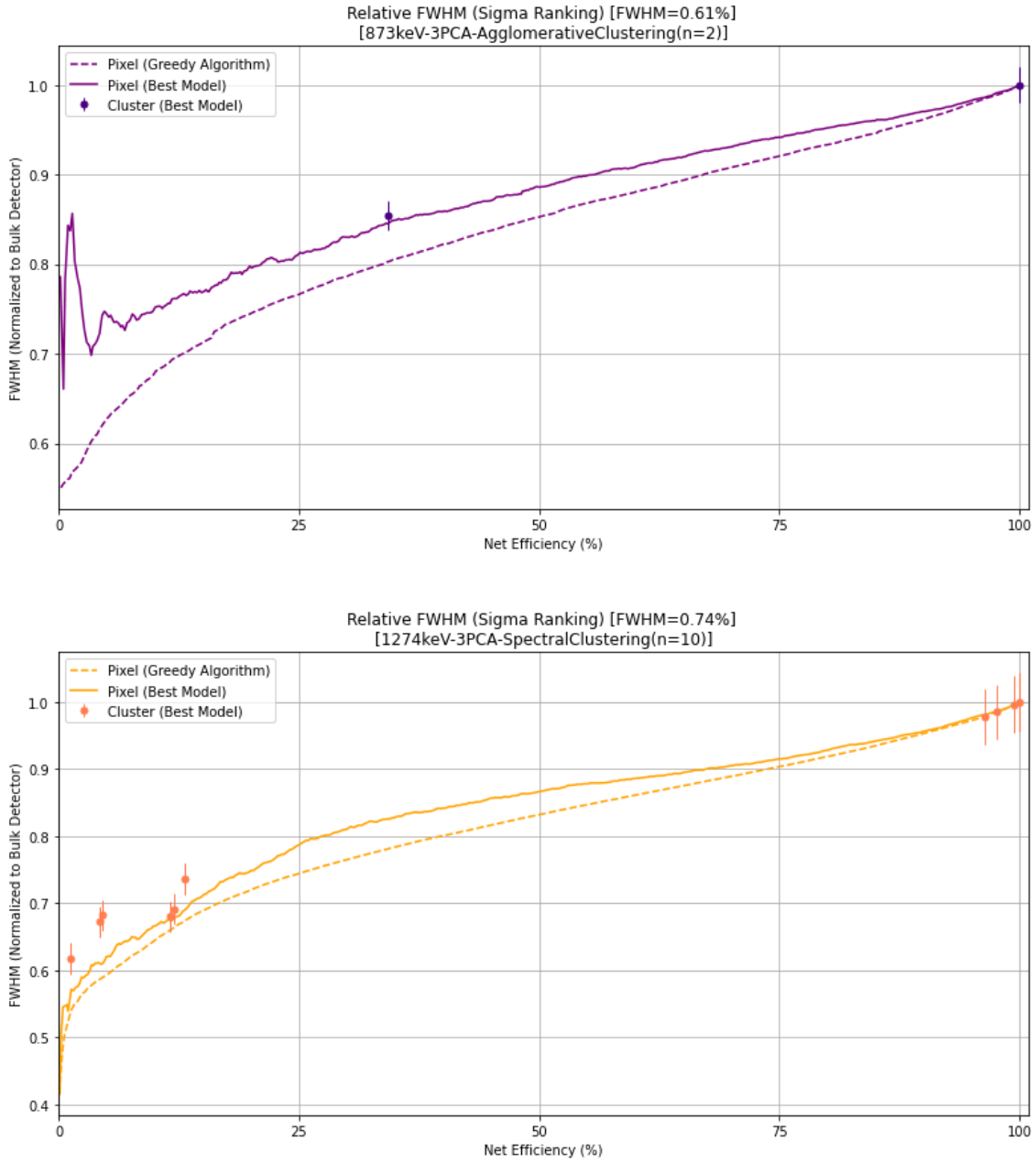

Figure 6. Relative FWHM for clusters (points) and pixels (solid line) ranked based on distance to optimal point in latent space compared to the greedy algorithm (dashed line).

The clustering approach is well aligned with the greedy algorithm demonstrating that the unsupervised learning approach can learn a latent representation of the data and cluster the pixels based on spectral performance. However, the top pixels, based on distance to the optimal point in the latent space, are very poor for 248 and 723 keV scenarios. This was determined to be partially explained by the anisotropic nature of

the Doniach sigma within the latent space (Fig. 7). An improved approach is to use a ratio of cluster sigma to optimal sigma or to simply rank based on the lowest cluster sigma. Moreover, a new *resolvability* metric [24] has been constructed to better quantify the separability of overlapping peaks. Additional comparative analysis is recommended to study the stability and applicability of different clustering algorithms.

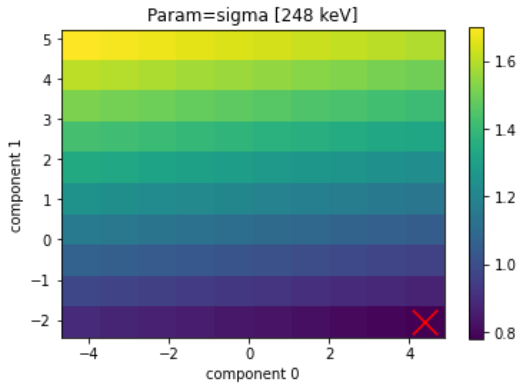

Figure 7. Distribution of sigma within a 2-PCA latent space (248 keV) showing the anisotropic behavior with larger gradients in the component1-direction. The optimal point is marked with a large, red X.

Removing detector voxels prior to detector pixels may improve the performance of the unsupervised learning algorithm because poor performing voxels degrade the pixel performance as they are accumulated. An adjacent study under this project shows clear patterns around the anode and edges of the detector [24] which can be removed prior to clustering the detector voxels. Moreover, the data in this work was averaged over measurements preformed at various angles around the source which could be hiding angular response patterns of the detector.

The worst clusters were successively removed until the relative detector net efficiency (with background subtracted) was below 50% demonstrating how an Inspector can trade-off detector efficiency for improved resolution in the field. Figure 8

shows the resulting pixel masks with bright pixels ‘on’ and dark pixels ‘off’ for each of the four photopeaks. The resulting net efficiency was 33.43%, 43.74%, 16.07%, and 13.07% respectively. The large variation is due to differences in the number of pixels per cluster and the total detector counts per cluster. For lower energies, the edges of the detector are low performing potentially due to shielding effects where the edges are preferred for the higher energy photopeaks.

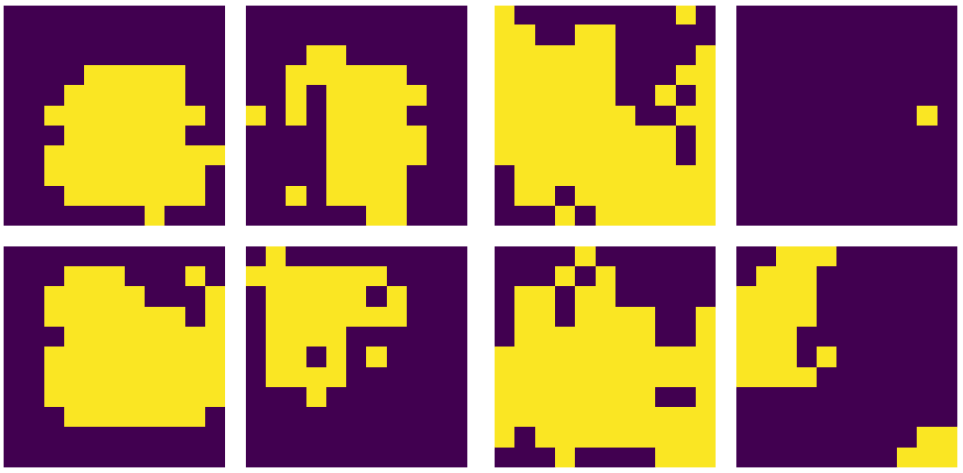

123 keV 248 keV

723 keV 1274 keV

Figure 8. Pixel masks with the worst clusters removed for 123 keV/248 keV (top left, top right) and 723 keV/1274 keV (bottom left, bottom right).

3.3 Application on Uranium Standards

The 123 keV model was applied to spectra data obtained from U_3O_8 standards measurements at Lawrence Berkeley National Laboratory to demonstrate that the model can generalize on newly seen spectra (Fig. 9). Here, the worst 100 and 200 pixels were removed resulting in 78% and 59% detector efficiency. The photopeaks demonstrate better visual spectral characteristics (background reduced and narrower peaks). However, quantification of the improvement is still ongoing.

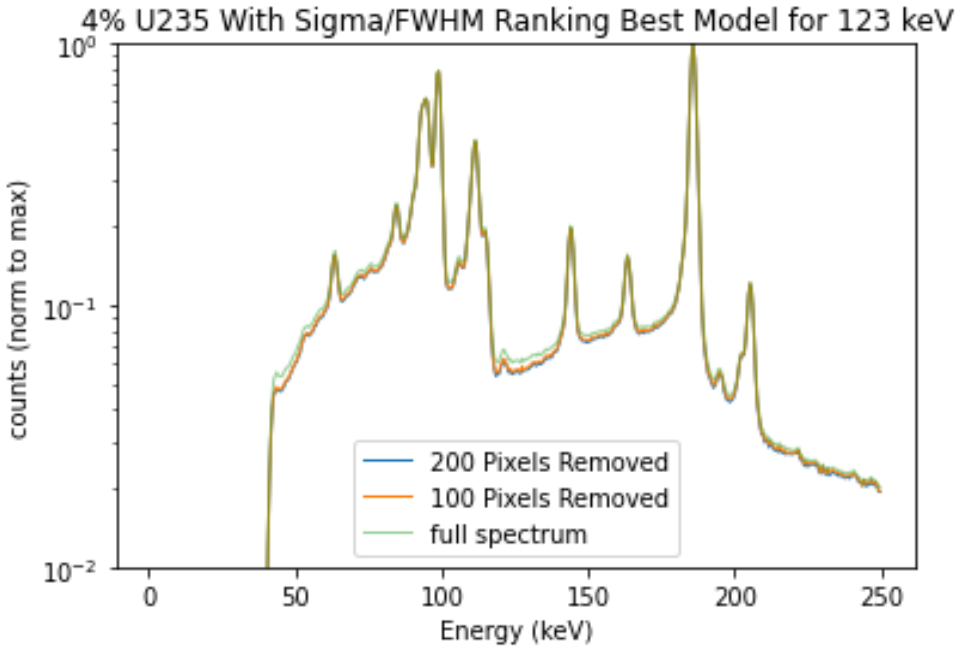

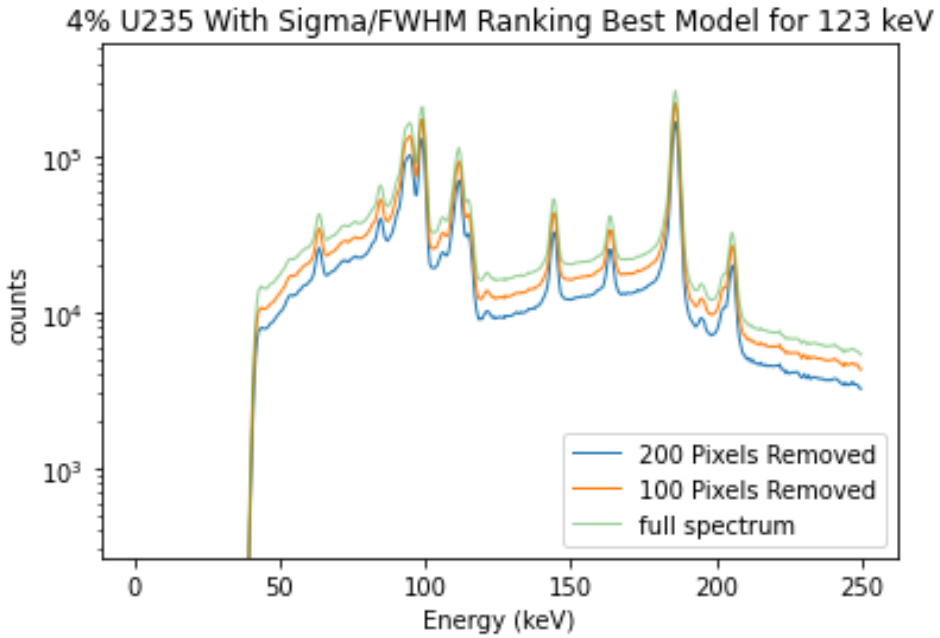

Figure 9. Pixel removal using a 4-PCA-component model on a 4% enriched U_3O_8 standard. (Top) spectra are normalized to their maxima, to show the changes in shape as the worst pixels are removed.

It is possible that differences between the measurement configuration for the Eu-154 training data and U_3O_8 resulted in an overfitted model. The uranium measurement was conducted at a 1 cm standoff distance to accommodate the shielding of the container. The detector response as a function of energy and measurement time should be constant. However, shielding and attenuation through air may contribute to individual pixel performance. Averaging spectra over several angular measurements when training the model may have also contributed to overfitting since the uranium measurements were taken head-on only.

4. CONCLUSIONS & FUTURE WORK

Unsupervised learning algorithms show promise to improve detector resolution by learning and rejecting poorly performing regions of the detector. By reducing the net

efficiency by 50%, the FWHM can be improved by 10-15%. This technique is particularly useful when analyzing peaks that are not well-separated, as improvements in FWHM are, in this case, often more valuable for reducing peak area uncertainties than the corresponding loss in efficiency.

The proposed approach provides a new solution, that is detector agnostic, to cluster and subsequently remove poor performing pixels to improve spectral performance. Operators can span the efficiency-resolution tradeoff in real-time in the field giving them the required flexibility for different safeguard related inspections. These capabilities will be released as a software package, including the ability to use other unsupervised learning algorithms and customize the ranking process [24], in the near future.

The preliminary evaluation in this work uses a Figure of Merit to compare the results of PCA and clustering against a greedy algorithm to assert whether the formed clusters pertain to spectral performance as intended. The current approach aligns well with, but does not outperform, the greedy algorithm which accumulates pixels based on best spectral performance. By removing the "worst" clusters, based on distance to optimal point in the latent space, the FWHM was incrementally improved. In future work, characterization of the clusters (based on, for example, FWHM or other spectral characteristics) should be conducted to develop a deeper interpretation of the results.

The approach presented in this work can be extended to include features from multiple photopeaks and source directions to better understand the capabilities of unsupervised learning for this application. Initial prototyping has shown promise in a multi-energy model that can in fact outperform the greedy algorithm. However, additional hyperparameters and model feature combinations need to be explored, compared, and evaluated. The clustering ranking based on distance to an optimal point

in the learned latent space was problematic due to the anisotropic nature of the ranking metric. Instead, the cluster accumulated metric (FWHM or resolvability) can be used to rank the clusters. Finally, clustering can be conducted at the voxel level for improved discretization of the detector [24].

ACKNOWLEDGEMENTS

The work presented in this paper was funded by the National Nuclear Security Administration of the Department of Energy, Office of International Nuclear Safeguards. This work was performed under the auspices of the U.S. Department of Energy by Lawrence Berkeley National Laboratory (LBNL) under Contract DE-AC02-05CH11231.

REFERENCES

1. W. KAYE, M. STREICHER, and F. ZHANG, "In-Situ Sample Analysis with Portable Gamma Spectrometers," Proceedings of the 15th International Congress of the International Radiation Protection Association, (2015).
2. "Development and Implementation Support Programme for Nuclear Verification 2022-2023," IAEA Safeguards Report STR-393, (2022).
3. "M400, Custom Integrable Detector Module," H3D Inc., https://h3dgamma.com/M400Specs.pdf, (current as of Aug. 1, 2023).
4. W. LI et al., "Spatial Variation of Energy Resolution in 3-D Position Sensitive CZT Gamma-ray Spectrometers", *IEEE Transaction on Nuclear Science*, **46,** 3, p. 628-633, (1999). https://doi.org/10.1109/NSSMIC.1998.775218.
5. F. ANOWAR, S. SADAOUI, and B. SELIM, "Conceptual and empirical comparison of dimensionality reduction algorithms (PCA, KPCA, LDA, MDS, SVD, LLE, ISOMAP, LE, ICA, t-SNE)," *Computer Science Review*, **40**, (2021). https://doi.org/10.1016/j.cosrev.2021.100378.
6. D. D. LEE and H. S. SEUNG, "Learning the Parts of Objects by Non-negative Matrix Factorization", *Nature*, **401**, p. 788–791, (1999). https://doi.org/10.1038/44565.
7. M. S. BANDSTRA et al., "Modeling Aerial Gamma-Ray Backgrounds Using Non-negative Matrix Factorization", *IEEE Transaction on Nuclear Science*, **67**, 5, p. 777-790, (2020). https://doi.org/10.1109/TNS.2020.2978798.
8. I.T. JOLLIFE and J. CADIMA, "Principal component analysis: a review and recent developments," *Philosophical Transactions of the Royal Society A.,* **374**, (2016). https://doi.org/10.1098/rsta.2015.0202.
9. T. ALHARBI, "Principal Component Analysis for pulse-shape discrimination of scintillation radiation detectors," *Nuclear Instruments and Methods in Physics Research Section A: Accelerators, Spectrometers, Detectors and Associated Equipment*, **806**, p. 240-243 (2016). https://doi.org/10.1016/j.nima.2015.10.030.

10. D. BOARDMAN, M. REINHARD and A. FLYNN, "Principal Component Analysis of Gamma-Ray Spectra for Radiation Portal Monitors," *IEEE Transactions on Nuclear Science*, **59,** 1, p. 154-160, (2012). https://doi.org/10.1109/TNS.2011.2179313.
11. K. M. GORSKI et al., "HEALPix: A Framework for High-Resolution Discretization and Fast Analysis of Data Distributed on the Sphere," *The Astrophysical Journal*, **662**, (2005). https://doi.org/10.1086/427976.
12. S. DONIACH and M. SUNJIC, "Many-electron Singularity in X-ray Photoemission and X-ray Line Spectra from Metals," *Journal of Physics C: Solid State Phys*ics, **3**, 2, (1970). https://doi.org/10.1088/0022-3719/3/2/010.
13. F. PEDREGOSA et al., "Scikit-learn: Machine Learning in Python," *Journal of Machine Learning Reaching*, **12**, p. 2825-2830, (2011). https://dl.acm.org/doi/10.5555/1953048.2078195.
14. T. ZHANG, R. RAMAKRISHNAN, and M. LIVNY, "BIRCH: An Efficient Data Clustering Method for Very Large Databases," *ACM SIGMOID Record*, **25**, 2, p. 103-114, (1996). https://doi.org/10.1145/235968.233324.
15. A. S. VIJAYA and R. BATEJA, "A Review on Hierarchical Clustering Algorithms," *Journal of Engineering and Applied Sciences*, **12**, 24, p. 7501-7507, (2017). doi:10.36478/jeasci.2017.7501.7507.
16. J. HARTIGAN and M. WONG, "Algorithm AS136: A k-means clustering algorithm," *Journal of Royal Statistical Society (Applied Statistics)*, **28**, 1, p. 100-108, (1979). https://doi.org/10.2307/2346830.
17. M. ESTER, et al., "A Density-Based Algorithm for Discovering Clusters in Large Spatial Databases with Noise," Proceedings of the 2nd International Conference on Knowledge Discovery and Data Mining, AAAI Press, p. 226–231, (1996). doi:10.5555/3001460.3001507.
18. M. ANKERST, et al., "OPTICS: ordering points to identify the clustering structure," *ACM Sigmod Record*, **28**, 2, p. 49-60. (1999). https://doi.org/10.1145/304181.304187.
19. C. BOUVEYRON, S. GIRARD, and C. SCHMID, "High-dimensional data clustering", *Computational Statistics & Data Analysis*, **52**, 1, p. 502-519, (2007). https://doi.org/10.1016/j.csda.2007.02.009.
20. B. J. FREY and D. DUECK, "Clustering by Passing Messages Between Data Points," *Science*, **315**, 5814, p. 972-976, (2007). http://dx.doi.org/10.1126/science.1136800.
21. YU, and SHI, "Multiclass spectral clustering," Proceedings Ninth IEEE International Conference on Computer Vision, Nice, France, **1**, p. 313-319, (2003) http://doi.org/10.1109/ICCV.2003.1238361.
22. D. COMANICIU and P. MEER, "Mean shift: A robust approach toward feature space analysis," *IEEE Transactions on Pattern Analysis and Machine Intelligence*, **24**, 5, p. 603-619, (2002). http://doi.org/10.1109/34.1000236.
23. R. GELBARD, O. GOLDMAN, and I. SPIEGLER, "Investigating diversity of clustering methods: An empirical comparison," *Data & Knowledge Engineering*, **63**, 1, p. 155-166, (2007). https://doi.org/10.1016/j.datak.2007.01.002.
24. G. AVERSANO, et al., "Data-Drive Event Selection in Pixelated Cadmium Zinc Telluride (CZT) Detectors for Improved Gamma-Ray Spectrometry," Proceedings INMM Annual Meeting, (2023).